Full Paper

CONTRAST MEDIA & MOLECULAR IMAGING

Received: 12 October 2009, Revised: 5 April 2010, Accepted: 9 April 2010, Published online in Wiley Online Library: 20 July 2010

(wileyonlinelibrary.com) DOI:10.1002/cmmi.390

Background migration of USPIO/MLs is a major drawback for *in situ* labeling of endogenous neural progenitor cells

Ruth Vreys[a], Stefaan J. H. Soenen[b], Marcel De Cuyper[b] and Annemie Van der Linden[a]*

MR-labeling of endogenous neural progenitor cells (NPCs) to follow up cellular migration with *in vivo* magnetic resonance imaging (MRI) is a very promising tool in the rapidly growing field of cellular imaging. To date, most of the *in situ* labeling work has been performed using micron-sized iron oxide particles. In this work magnetoliposomes (MLs), i.e. ultrasmall superparamagnetic iron oxide cores (USPIOs), each individually coated by a phospholipid bilayer, were used as the MR contrast agent. One of the main advantages of MLs is that the phospholipid bilayer allows easy modification of the surface, which creates the opportunity to construct a wide range of MLs optimized for specific biomedical applications. We have investigated the ability of MLs to label endogenous NPCs after direct injection into the adult mouse brain. Whereas MRI revealed contrast relocation towards the olfactory bulb, our data strongly imply that this relocation is independent of the migration of endogenous NPCs but represents background migration of MLs along a white matter tract. Our findings suggest that the small size of USPIOs/MLs intrinsically limits their potential for *in situ* labeling of NPCs. Copyright © 2010 John Wiley & Sons, Ltd.

Keywords: magnetic resonance imaging; magnetoliposomes; *in situ* cell labeling; white matter; contrast agents; USPIOs

1. INTRODUCTION

Nowadays, there is an increased interest in a reliable *in vivo* non-invasive method to monitor migration of endogenous stem cells in the adult brain. Magnetic resonance imaging (MRI) has gained a substantial position in cellular imaging during recent decades. Whereas MRI has excellent soft tissue contrast and high *in vivo* spatial resolution, cells of interest need to be magnetically labeled in order to distinguish them from the surrounding tissues. Initial studies on *in situ* labeling of endogenous neural progenitor cells (NPCs) in the adult rodent brain have been performed using micron-sized superparamagnetic iron oxide particles (MPIOs) (1,2). These studies showed that intraventricular injection of MPIOs resulted in successful labeling of endogenous NPCs and that the migration of MPIO-labeled NPCs can be visualized with *in vivo* MRI. Nonetheless, this labeling strategy suffers from several limitations. A large number of injected particles is necessary to achieve adequate cell labeling, which results in a large signal loss and consequently in a distortion of the MR images. In addition, the uptake of MPIOs after intraventricular injection is rather small (up to 30% of all migrating cells were labeled) (1,2). In a previous study of our group, efforts to optimize the *in situ* labeling technique with MPIOs showed successful labeling of endogenous NPCs after intraventricular injection of a small number of MPIOs (9.1×10^5 particles, 0.67 mg Fe/ml) in combination with the transfection agent poly-L-lysine (3). In the same study, we reported an alternative strategy to achieve *in situ* labeling of NPCs: direct injection of a small number of MPIOs in the brain parenchyma near the rostral migratory stream (RMS). However, despite the notable labeling capacity of MPIOs, it seemed that the normal migration process of NPCs was impeded by the MPIOs (3). It has been previously suggested that the large particle size of the MPIOs may interfere with normal cellular processes (4).

In this work, magnetoliposomes (MLs) were chosen as contrast agent for *in situ* cell labeling. MLs are phospholipid-coated ultrasmall (nano-sized) superparamagnetic iron oxide particles (USPIOs) that have already been used in a wide range of prominent biomedical research [for a review see Soenen *et al.* (5)]. One important benefit of MLs is that surface modification can be

* *Correspondence to: A. Van der Linden, Universiteit Antwerpen, Bio Imaging Lab Groenenborgerlaan 171, B-2020 Antwerpen, Belgium. E-mail: Annemie.vanderlinden@ua.ac.be*

a *R. Vreys, A. Van der Linden*
Bio-Imaging Laboratory, Department of Biomedical Sciences, University of Antwerp, B-2020 Antwerp, Belgium

b *S. J. H. Soenen, M. De Cuyper*
Interdisciplinary Research Centre, Laboratory of BioNanoColloids, KULeuven – Campus Kortrijk, B-8500 Kortrijk, Belgium

Contract/grant sponsor: Institute for the Promotion of Innovation through Science and Technology in Flanders (IWT-Vlaanderen).
Contract/grant sponsor: SBO grants from the Flemish Institute; contract/grant number: IWT-030238: ANIMONE, IWT-60838: BRAINSTIM and IWT-80017: iMAGiNe.
Contract/grant sponsor: EC–FP6-poject DiMI; contract/grant number: LSHB-CT-2005-512146.
Contract/grant sponsor: EC–FP6-project EMIL; contract/grant number: LSHC-CT-2004-503569.
Contract/grant sponsor: Inter University Attraction Poles; contract/grant number: IUAP-NIMI-P6/38.

easily performed as the ML coating consists of a phospholipid bilayer which can be chemically modified to construct MLs with various surface properties. For instance, prolonged blood circulation of MLs after intravenous injection has been achieved by embedding PEGylated phospholipids in the ML coat (6). Recently, it has been shown *in vitro* that MLs are internalized by 3T3 fibroblasts and that cellular uptake of MLs can be significantly augmented when incorporating small percentages of cationic lipids into the ML coat; however, this increased internalization occurs at the risk of augmented toxicity of the particles, induced by the inherent toxic effects of the cationic lipids (7). Here we investigated the potential of MLs to label endogenous NPCs in healthy adult mice by direct injection of MLs (anionic, neutral or cationic) in the brain parenchyma near the RMS.

2. RESULTS AND DISCUSSION

Mice ($n = 6$) were injected with MLs (0.67 mg Fe/ml) in the brain parenchyma near the RMS. As soon as 1 week after *in situ* ML injection, we observed on *in vivo* MR images of four mice a hypointense line from the injection site into the core of the olfactory bulb (OB). Figure 1 shows *in vivo* MR images of two animals at 1 week post-injection (PI). The contrast relocation in the forebrain can be observed as a prominent hypointense line on *in vivo* 3D MR images. The insets in Fig. 1A and D show that even on *in vivo* axial 2D MR images contrast relocation was detectable as a faint hypointense line. Remarkably, in all four mice, the contrast relocation towards the OB faded at later MRI time points. Figure 2 shows minimum intensity projections (mIPs) of eight consecutive *in vivo* MRI sections of the forebrain of a mouse, clearly displaying contrast reversion during the MRI time course. While at 3 weeks PI (Fig. 2B) the hypointense line towards the OB was still visible, but less pronounced as at 1 week PI (Fig. 2A), the contrast relocation was almost undetectable at 8 weeks PI (Fig. 2C). Only in one animal were hypointense pixels still present in the core of the OB at 8 weeks PI (Fig. 3A). The *ex vivo* MR images confirmed the *in vivo* MRI results at 8 weeks PI (Fig. 3). From the four mice for which contrast reversion was shown, in one mouse, some hypointense pixels could be located at the level of the RMS and in the core of the OB (Fig. 3A and D), whereas for the other three animals, dark pixels at the level of the RMS were only visible close to the injection spot (Fig. 3B and E). No hypointense pixels were found in the RMS or OB on the MR images of the remaining two mice (Fig. 3C and F).

Besides the contrast relocation towards the OB, we observed on the MR images of one mouse other hypointense tracks starting from the injection site which were oriented posterior and lateral from the injection site (Fig. 4). These two hypointense tracks were already present at the first MRI measurement (1 week PI) and similar to the contrast relocation towards the OB, the contrast faded at later MRI time points (Fig. 4A and B). On the

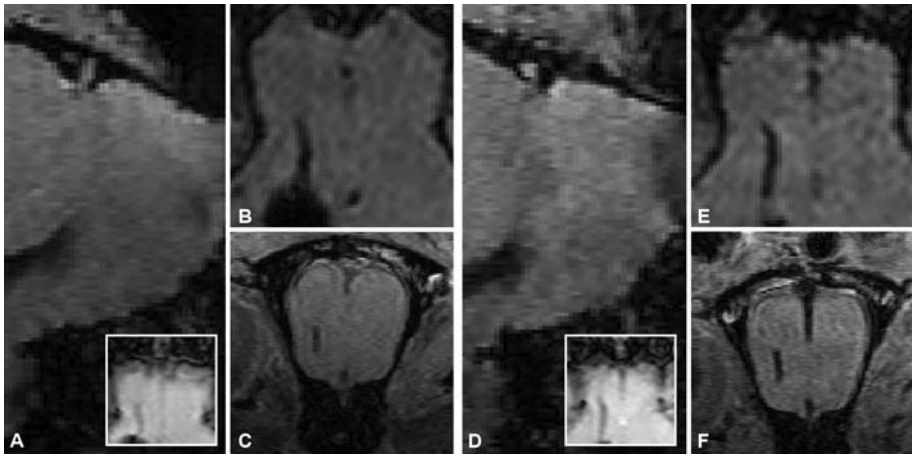

Figure 1. *In vivo* MRI at 1 week PI. (A–C) Sagittal, axial and coronal 3D GE MR images of a mouse injected with neutral MLs. (D–F) Sagittal, axial and coronal 3D GE MR images of a mouse injected with anionic MLs. In both animals a hypointense line is clearly visible in the forebrain and in the OB. Insets in (A) and (D) show the presence of a hypointense line on axial *in vivo* 2D GE MR images.

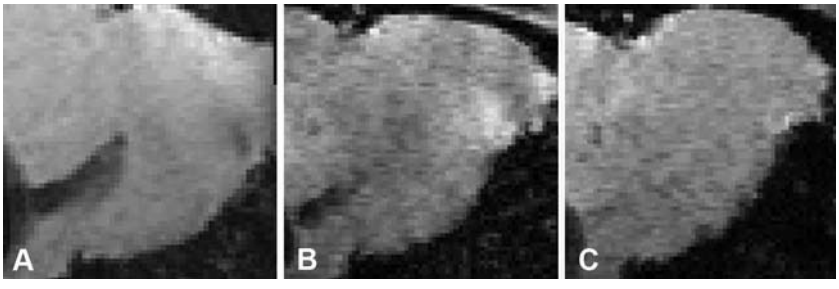

Figure 2. Longitudinal *in vivo* 3D GE MRI. For each time point of MRI a minimum intensity projection (mIP) of eight consecutive sagittal MR images at the level of the RMS from the same animal (injected with neutral MLs) is shown. (A) At 1 week PI, a prominent hypointense line is visible in the forebrain and OB. (B) At 3 weeks PI, the hypointense line is more limited to the forebrain. (C) At 8 week PI, the hypointense line almost totally disappeared compared with (A) and (B).

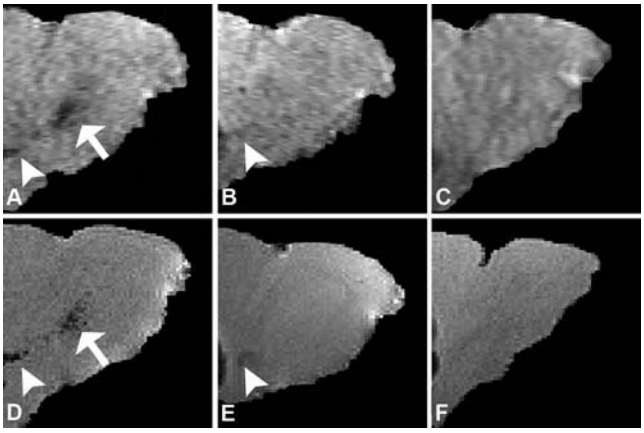

Figure 3. *In vivo* 3D GE sagittal MR images at 8 weeks PI (first row) and corresponding *ex vivo* 3D GE sagittal MR images (second row) of a mouse injected with anionic MLs (A and D), neutral MLs (B and E) and cationic MLs (C and F). White arrowheads indicate hypointense pixels at the level of the RMS. White arrows denote hypointense pixels in the OB.

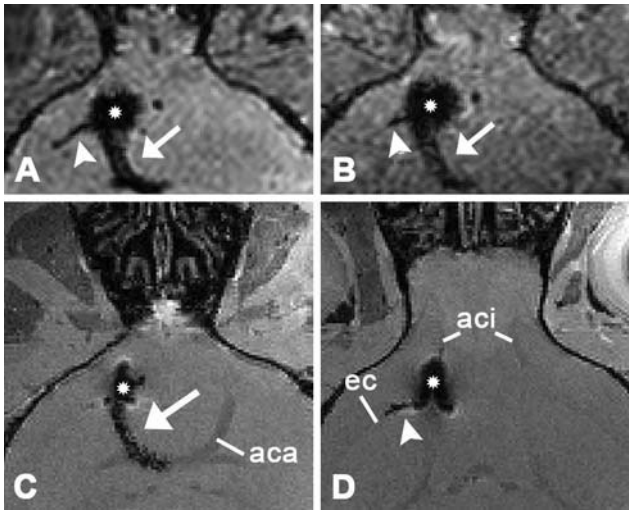

Figure 4. Additional contrast relocation routes. *In vivo* 3D GE axial MR image at 1 week PI (A) and 8 weeks PI (B) and *ex vivo* 3D GE axial MRI images (C and D) of a mouse injected with neutral MLs show the presence of hypointense tracks oriented lateral (white arrowheads) and posterior (white arrows) from the injection spot (asterix). aca, Anterior part of the anterior commissure; aci, interbulbar part of the anterior commissure; ec, external capsule.

ex vivo MR images, it can be clearly seen that the two additional hypointense tracks overlap with two white matter structures: the anterior part of the anterior commissure (aca) and the external capsule (ec) for the posterior and lateral relocation, respectively (Fig. 4C and D). This data suggests that MLs after direct injection in the mouse brain relocated along white matter tracts. As is already known, the RMS runs parallel with a white matter tract, namely the olfactory limb of the anterior commissure [or anterior commissure, interbulbar part (aci)] (8); hence, the contrast relocation towards the OB could represent relocation of MLs along this particular white matter tract.

In the adult rodent brain, thousands of newly formed NPCs enter the RMS per day to migrate towards the OB (9–11). This temporal process of tangential migration has a time span of 1–2 weeks (10,11). Once the NPCs arrive in the OB, they migrate radially into the granule cell layer and the periglomerular layer where they constantly replace interneurons (12). Previous work of our group demonstrated successful *in situ* labeling of endogenous NPCs after direct injection of MPIOs in the parenchyma close to the RMS (3). By comparing the contrast relocation towards the OB observed in ML-injected mice with the contrast relocation towards the OB observed in MPIO-injected mice, we notice two main differences. Firstly, contrast relocation over time differs considerably. Longitudinal MRI of mice injected with MPIOs revealed faint hypointense pixels towards the OB at 3 weeks PI and accumulation of dark pixels in the OB over time (up to 8 weeks PI) (3). In the study we report here, we observed the opposite, i.e. the largest amount of hypointense contrast towards the OB at the earliest time point (1 week PI) and contrast reversion at later time points (see Fig. 2). Secondly, the pattern of contrast relocation seen after *in situ* injection of MLs lacks resemblance with the pattern of migrating MPIO-labeled NPCs. Figure 5(A) shows a sagittal mIP of *in vivo* MRI at 3 weeks PI of a mouse injected with MPIOs. The contrast relocation can only be seen as a faint hypointense line at the level of the RMS and faint hypointense pixels are fanning out towards the edges of the OB. Figure 5(B) shows a sagittal mIP obtained from *in vivo* MRI at 3 weeks PI of a mouse injected with MLs. Here, a thick hypointense line marks the rostral part of the RMS and continues in the core of the OB where it stops abruptly. These apparent discrepancies strongly imply that the mechanism by which the MLs were relocated towards the OB is independent from the migration of endogenous NPCs towards the OB.

Prussian blue histology was performed to detect iron in the brain in order to validate the MRI observations. Prussian blue positive staining was observed at the injection site in all mice of this study. Figure 6(A) shows a coronal section at the injection site where iron staining can be observed along the injection track (white arrows) and at the injection spot (yellow box). Figure 6(B) shows migrating NPCs in the RMS (red fluorescence) adjacent to the Prussian blue positive injection spot. Surprisingly, Prussian blue staining was not completely compatible with the MRI data. Whereas hypointense contrast in the core of the OB was detected on the *ex vivo* MR images of one mouse (see Fig. 3D), no iron could be detected in Prussian blue-stained histological sections of the OB (data not shown). A study by Desestret and colleagues reported a similar failure to detect iron of USPIOs in

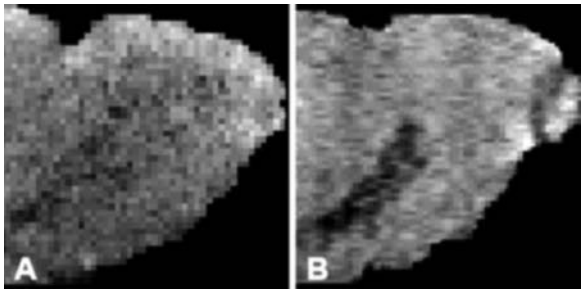

Figure 5. Sagittal minimum intensity projections (mIPs) of a subsample of *in vivo* 3D GE MRI at 3 weeks PI comprising the RMS of a mouse injected with MPIOs (A) and a mouse injected with anionic MLs (B). Differences in the pattern of contrast relocation can be observed when comparing (A) with (B). At the level of the RMS, the hypointense line is thicker and darker in (B) compared with (A). In the OB, highly punctuated dark areas spreading out into the OB can be seen in (A), whereas only a dark line that stops halfway along the OB is noticed in (B).

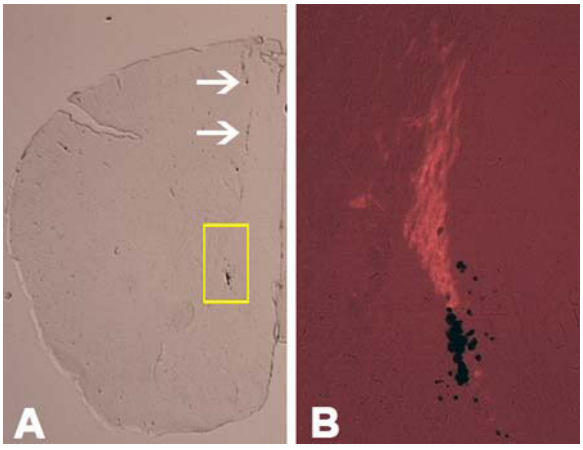

Figure 6. Prussian blue histology of a mouse injected with anionic MLs. (A) Coronal section at the level of the injection site shows Prussian blue-stained iron along the injection track (white arrows) and at the injection spot (yellow box). (B) Fluorescence microscopy at the level of the injection spot [magnification of the area in the yellow box in (A)] shows Prussian blue-stained iron adjacent to migrating NPCs in the RMS (red fluorescence).

the corpus callosum with Prussian blue histology while they showed a number of indirect indications of the presence of free USPIOs in the corpus callosum (13). It has been suggested that conventional Prussian blue staining may lack the sensitivity to detect interstitial USPIOs (13,14). Based on this assumption, our Prussian blue histology indicates that the contrast relocation observed on the MRI was due to migration of free interstitial MLs.

To sum up, our data indicate that the relocation of MLs towards the OB was not due to the migration of ML-labeled endogenous NPCs, but was rather a result of background migration of free MLs along a white matter tract. In line with our findings, the non-specific migration of free particles has also been described upon *in situ* injection of dextran-coated iron oxide particles into the brain parenchyma near the subventricular zone of adult rats (15), prohibiting any successful tracking of labeled NPCs into the OB with *in vivo* MRI at early time points.

Previous studies have provided evidence for the flow of brain interstitial fluid along preferential pathways, especially perivascular spaces and axon tracts [for a review see Abbott (16)]. The MLs used in our study have a particle size of 20 nm and hydrodynamic diameters of less than 50 nm (see Materials and Methods). The normal width of the extracellular matrix has been estimated as 38–64 nm (17). It is thus possible that ML migration was due to the flow of interstitial fluid in the extracellular matrix along white matter structures. As such, the small size of the MLs appears to intrinsically limit their use for *in situ* labeling of NPCs. For micron-sized particles, migration of the particles themselves will be hindered due to their large size, resulting in high levels of MPIOs, which remain localized in the injection spot (3). As a result, the uptake efficiency of these MPIOs (the number of particles taken up relative to the number of particles provided) can be rather low as the labeled, migrating cells can be specifically visualized based on distinctive alterations in signal localization against a static background (18). For nano-sized particles, this is far more difficult since, for efficient *in situ* labeling, an uptake efficiency of near 100% should be achieved, which is in practice highly improbable. For Endorem®, the uptake efficiency of the particles is only 1.74 and 1.59% in the case of mesenchymal stem cells and 3T6 fibroblasts, respectively (19). In optimal conditions, cationic lipid-containing MLs can have uptake efficiencies up to 20.9% in 3T3 fibroblasts (20). Although these values are obtained for *in vitro* 2D cell culture models, they are probably representative for the *in vivo* situation as well, suggesting that the majority of the particles will not be taken up by neighboring cells. Any particles which are not taken up by cells near the injection site will be able to travel along white matter tracts.

The fact that we did not observe contrast relocation for all animals might be explained by the different liposome composition of the MLs. Mice were injected with three different types of MLs: neutral ($n = 2$), anionic ($n = 2$) or cationic ($n = 2$) MLs. From the four mice displaying contrast relocation, two were injected with neutral MLs and two with anionic MLs, but none of the mice injected with cationic MLs showed contrast relocation although the injections were accurate. The latter observation might be explained by two mechanisms which are probably involved:

(1) A previous study on the technique of convection-enhanced delivery using liposomes for the delivery of agents in a large volume of brain tissue demonstrated that cationic liposomes display higher tissue affinity compared with neutral liposomes, leading to a significantly lower tissue diffusion of the positively charged liposomes (21). It is well known that cationic lipids show an electrostatic interaction with large negatively charged domains on cell membranes. As a result, cationic lipids are commonly applied to improve cellular uptake. It has been shown that the introduction of a cationic lipid in the outer layer of MLs resulted in a more efficient uptake of MLs by 3T3 fibroblasts *in vitro* (7).

(2) Because of their high surface charge, the cationic MLs are probably adsorbed by proteins, resulting in a so-called protein–corona structure (22). The formation of a protein corona is highly dependent on the charge and the charge density present on a particle surface and has been described to be maximal in the case of cationic particles. In addition, the latter are generally unstable in physiological media and are prone to aggregation, as has also been described for Resovist® in combination with cationic transfection agents (23,24).

As a result, the lower tissue diffusion together with the increase in size due to protein adsorption and formation of tiny aggregates probably impede any passive diffusion of the cationic MLs along white matter tracts.

3. CONCLUSIONS

The findings in the current study show that direct injection of MLs near the RMS did not succeed in labeling endogenous NPCs. Our results imply that USPIO/MLs have to be further optimized with regard to uptake efficiencies in order to be suitable for *in situ* cell labeling strategies. Furthermore, this work highlights a potential pitfall in cellular imaging of endogenous cells using direct injection of MR contrast agents. Contrast relocation observed with MRI can be misinterpreted as cellular recruitment whereas it represents background migration of the contrast agent independent from the migration of the cells of interest. As a valuable alternative, we would suggest the use of larger (extruded) MLs (diameter of 100–200 nm) containing cationic lipids below toxic levels.

4. MATERIALS AND METHODS

4.1. Animals

Six male adult C57BL/6J mice (12 weeks old, Charles River Laboratories, L'Arbresle cedex, France) were used in this study. Data from MPIO-injected male adult C57BL/6J mice (3) were included and are displayed in this study as reference material. All aspects of animal experiments were carried out in compliance with national and European regulations and were approved by the Animal Care and Use Committees of the University of Antwerp.

4.2. Unilateral stereotactic injection

Mice were anesthetized intraperitoneally with ketamine (Ketalar®: 50 mg/ml; Pfizer NV/SA, Brussels, Belgium) and medetomidine (Domitor®: 1 mg/ml; Pfizer Animal Health s.a., Louvain-la-Neuve, Belgium), and positioned in a stereotactic head frame. For the injection, a Hamilton syringe (26S Gage, VWR International, Haasrode, Belgium) was mounted on a pump and connected to a glass microcapillary to inject 1.5 μl at a constant rate of 0.50 μl/min. All mice were injected in the brain parenchyma near the RMS (left hemisphere) at the following stereotactic coordinates (relative to bregma): AP +1.7 mm, LM +0.7 mm, DV −4.1 mm. After injection, the capillary was left in place for an additional 5 min and then slowly withdrawn. After surgery, anesthesia was reversed using atipamezol (Antisedan®: 5 mg/ml, Pfizer Animal Health s.a., Louvain-la-Neuve, Belgium), which was administered intraperitoneally.

As contrast agent we used customized nano-sized MLs. MLs were injected within 2 days after preparation. Prior to injection, the MLs were diluted with a 5% glucose solution to a final concentration of 0.67 mg Fe/ml. For the MPIOs-injected mice, commercially purchased 1.63 μm diameter fluorescent MPIOs (3.00 mg Fe/ml, polystyrene/divinylbenzene-coated, green fluorescent dye: 480 nm excitation and 520 nm emission; Bangs Laboratories, Fishers, IN, USA) were used as contrast agent. MPIOs were diluted with 0.9% sodium chloride solution to a final concentration of 0.67 mg Fe/ml (3).

4.3. Magnetoliposome preparation and characterization

For this study three differently charged MLs (neutral, anionic and cationic MLs) were constructed. Neutral and anionic MLs were prepared as described previously (25), using dimyristoylphosphatidylcholine (DMPC) as the neutral matrix lipid and 90% DMPC and 10% dimyristoylphosphatidylglycerol (DMPG) for the anionic MLs. Cationic MLs were prepared in a two-step procedure, starting from neutral DMPC MLs which were incubated with an equimolar amount of vesicles (50% 1,2-dioleoyl-3-trimethylammonium propane (DOTAP)–50% DMPC, molar ratio), followed by high-gradient magnetophoresis as described previously (26). After magnetic fractionation, the resulting MLs were suspended in phosphate-buffered saline (PBS) after which the iron and phosphate concentrations of the purified ML solutions were determined as described in Soenen *et al*. (27) (neutral ML solution: 17.15 mg Fe/ml; anionic ML solution, 11.19 mg Fe/ml, and cationic ML solution, 10.54 mg Fe/ml). Next, the size of the iron oxide cores (14.0 ± 0.3 nm diameter for all samples) was determined by transmission electron microscopy; the electrophoretic mobilities were measured with a Zetasizer IIC instrument (Malvern, UK) at 25°C and hydrodynamic radii were determined by a PCS 100 spectrometer (Malvern, UK) at 25°C, measuring the scattered light at a 90° angle, as described previously (20). For anionic, neutral and cationic MLs, hydrodynamic radii of 19.24 ± 1.67, 22.62 ± 1.99 and 24.98 ± 2.42 nm, respectively, and ζ-potentials of -31.23 ± 3.61, -8.39 ± 2.78 and +62.42 ± 5.21 mV, respectively, were obtained.

4.4. Magnetic resonance imaging

In vivo MRI was performed at 300 MHz on a 7 T magnet from Magnex Scientific (Oxfordshire, UK) with a console from MR Solutions (Guildford, UK). A Helmholtz volume transmit antenna (50 mm) and actively decoupled surface receiving antenna (20 mm) were used. Animals were imaged 1 week, 3 weeks and 8 weeks PI. During MRI, the mice were anesthetized by isoflurane (Isoflo®; 3% for induction and 1% for maintenance) in a mixture of 30% O_2 and 70% N_2 at a flow rate of 600 ml/min. Breathing rate (110 ± 10 breaths/min) and body temperature (37 ± 0.5°C) were continuously monitored with pcsam software (SA Instrument rents, NY, USA). Two-dimensional multislice coronal and sagittal T_2*-weighted images were acquired with a 2D gradient echo (GE) sequence using the following image parameters: *TR*/*TE* = 500/6 ms, FOV = 20 mm, matrix = 256*128, slice thickness = 1 mm. Three-dimensional axial T_2*-weighted images were acquired with a 3D GE sequence using the following image parameters: *TR*/*TE* = 500/6 ms, averages = 1; FOV = 20 × 20 × 6.5 mm (1 week PI) or 14 × 14 × 6.5 mm, matrix = 256 × 128 × 64.

All animals were sacrificed at 12 weeks PI with an intraperitoneal overdose of pentobarbital (Nembutal®; CEVA Santé Animale, Brussels, Belgium). Animals were transcardially perfused with 4% paraformaldehyde (PFA) in 0.1 M PBS (pH 7.4) doped with 1 mM Gd–DOTA. The whole mouse head was fixed overnight in 4% PFA at 4°C prior to transfer to PBS. *Ex vivo* MRI was performed on all subjects. The fixed mouse head was covered with Parafilm® and placed in the stereotactic device in the same orientation as a living mouse. High-resolution 3D coronal GE images were obtained with the following image parameters: *TR*/*TE* = 100/6.3 ms, FOV = 17 × 17 × 17 mm (covering the whole mouse brain), matrix = 256 × 256 × 256 (66 μm isotropic voxel size) and averages = 6, with a total scanning time of approximately 10 h 56 min.

4.5. Post-processing of MR images

For post-processing, Amira software (version 4.0.1, Mercury Computers Systems, CA, USA) was used. Minimum intensity projections (mIPs) were created from a subsample of sagittal slices of *in vivo* 3D MRI covering the brain region that contains the RMS.

4.6. Histology

After *ex vivo* MRI, the brains were removed from the skulls and serial 50 μm coronal sections were made with a microtome (Vibratome, St Louis, MO, USA). Prussian blue staining was performed to detect the iron oxide of the MLs. Sections were immersed in 20% hydrochloric acid and 10% potassium ferrocyanide for 20 min at 56°C, then washed in distilled water. Finally, after dehydration in 95% ethanol sections were mounted using DPX mountant.

Every third section was used for immunohistochemistry. Double immunofluorescence stainings were done overnight at

room temperature in PBS-10% horse serum (v/v)–0.1% Triton (v/v) with the following antibodies: goat anti-doublecortin (Dcx) as a marker for migrating NPCs (1:200; Santa Cruz Biotechnology, Heidelberg, Germany) and mouse anti-neuronal nuclear antigen (NeuN) for labeling of mature neurons (1:200; Chemicon International, Heule, Belgium). The next day, sections were incubated with the following fluorescently labeled secondary antibodies at room temperature for 2 h: donkey anti-goat-Alexa 555 (1:300; Molecular Probes, Leiden, The Netherlands) and donkey anti-mouse-Alexa 647 (1:300; Molecular Probes). Sections were mounted on glass slides, coverslipped with polyvinyl alcohol/1,4-diazabicyclo-[2.2.2]octa (PVA-DABCO) (Fluka; Sigma-Aldrich). Fluorescence images were obtained on a fluorescence microscope (Leica DMR Biopoint 2; Leica Microsystems, Wetzlar, Germany) and a laser scanning confocal microscope (LSM510; Carl Zeiss, Oberkochen, Germany).

Acknowledgements

We are highly grateful to M. Geraerts for her assistance with the histology work. R. Vreys and S. J. H. Soenen are funded by PhD grants from the Institute for the Promotion of Innovation through Science and Technology in Flanders (IWT-Vlaanderen). This work was funded in part by SBO grants (IWT-030238: ANIMONE, IWT-60838: BRAINSTIM and IWT-80017: iMAGiNe) from the Flemish Institute supporting scientific-technological research in industry (IWT), by the EC–FP6-poject DiMI (LSHB-CT-2005-512146), by the EC – FP6-project EMIL (LSHC-CT-2004-503569), and by the Inter University Attraction Poles (IUAP-NIMI-P6/38).

REFERENCES

1. Shapiro EM, Gonzalez-Perez O, Garcia-Verdugo JM, Alvarez-Buylla A, Koretsky AP. Magnetic resonance imaging of the migration of neuronal precursors generated in the adult rodent brain. NeuroImage 2006; 32: 1150–1157; doi:10.1016/j.neuroimage.2006.04.219
2. Sumner JP, Shapiro EM, Maric D, Conroy R, Koretsky AP. In vivo labeling of adult neural progenitors for MRI with micron sized particles of iron oxide: quantification of labeled cell phenotype. NeuroImage 2009; 44: 671–678; doi:10.1016/j.neuroimage.2008.07.050
3. Vreys R, Vande Velde G, Krylychkina O, *et al*. MRI visualization of endogenous neural progenitor cell migration along the RMS in the adult mouse brain: validation of various MPIO labeling strategies. NeuroImage 2010; 49: 2094–2103; doi:10.1016/j.neuroimage.2009.10.034
4. Modo M, Hoehn M, Bulte JW. Cellular MR imaging. Mol Imaging 2005; 4: 143–164.
5. Soenen SJ, Hodenius M, De Cuyper M. Magnetoliposomes: versatile innovative nanocolloids for use in biotechnology and biomedicine. Nanomedicine 2009; 4: 177–191; doi:10.2217/17435889.4.2.177
6. Bulte JW, De Cuyper M, Despres D, Frank JA. Short- vs. long-circulating magnetoliposomes as bone marrow-seeking MR contrast agents. J Magn Reson Imaging 1999; 9: 329–335.
7. Soenen SJ, Baert J, De Cuyper M. Optimal conditions for labelling of 3T3 fibroblasts with magnetoliposomes without affecting cellular viability. Chembiochem 2007; 8: 2067–2077; doi:10.1002/cbic.200700327
8. Brunjes PC, Illig KR, Meyer EA. A field guide to the anterior olfactory nucleus (cortex). Brain Res Rev 2005; 50: 305–335; doi:10.1016/j.brainresrev.2005.08.005
9. Alvarez-Buylla A, Garcia-Verdugo JM, Tramontin AD. A unified hypothesis on the lineage of neural stem cells. Nat Rev Neurosci 2001; 2: 287–293; doi:10.1038/35067582
10. Lois C, Alvarez-Buylla A. Long-distance neuronal migration in the adult mammalian brain. Science 1994; 264: 1145–1148; doi:10.1126/science.8178174
11. Luskin MB. Restricted proliferation and migration of postnatally generated neurons derived from the forebrain subventricular zone. Neuron 1993; 11: 173–189; doi:10.1016/0896-6273(93)90281-U
12. Kato T, Yokouchi K, Fukushima N, Kawagishi K, Li Z, Moriizumi T. Continual replacement of newly-generated olfactory neurons in adult rats. Neurosci Lett 2001; 307: 17–20; doi:10.1016/S0304-3940(01)01914-0
13. Desestret V, Brisset JC, Moucharrafie S, *et al*. Early-stage investigations of ultrasmall superparamagnetic iron oxide-induced signal change after permanent middle cerebral artery occlusion in mice. Stroke 2009; 40: 1834–1841; doi:10.1161/STROKEAHA.108.531269
14. Rausch M, Baumann D, Neubacher U, Rudin M. In-vivo visualization of phagocytotic cells in rat brains after transient ischemia by USPIO. NMR Biomed 2002; 15: 278–283; doi:10.1002/nbm.770
15. Justicia C, Himmelreich U, Ramos-Cabrer P, Sprenger C, Hoehn M. In vivo tracking of endogenous stem cells by MRI after intraparenchymal injection of iron oxide nanoparticles. Mol Imag 2005; 4: 351–352.
16. Abbott NJ. Evidence for bulk flow of brain interstitial fluid: significance for physiology and pathology. Neurochem Int 2004; 45: 545–552; doi:10.1016/j.neuint.2003.11.006
17. Thorne RG, Nicholson C. In vivo diffusion analysis with quantum dots and dextrans predicts the width of brain extracellular space. Proc Natl Acad Sci USA 2006; 103: 5567–5572; doi:10.1073/pnas.0509425103
18. Hoehn M, Wiedermann D, Justicia C, *et al*. Cell tracking using magnetic resonance imaging. J Physiol 2007; 584: 25–30; doi:10.1113/jphysiol.2007.139451
19. Boutry S, Brunin S, Mahieu I, Laurent S, Vander Elst L, Muller RN. Magnetic labeling of non-phagocytic adherent cells with iron oxide nanoparticles: a comprehensive study. Contrast Media Mol Imag 2008; 3: 223–232; doi:10.1002/cmmi.256
20. Soenen SJ, Illyes E, Vercauteren D, *et al*. The role of nanoparticle concentration-dependent induction of cellular stress in the internalization of non-toxic cationic magnetoliposomes. Biomaterials 2009; 30: 6803–6813; doi:10.1016/j.biomaterials.2009.08.050
21. Saito R, Krauze MT, Noble CO, *et al*. Tissue affinity of the infusate affects the distribution volume during convection-enhanced delivery into rodent brains: implications for local drug delivery. J Neurosci Meth 2006; 154: 225–232; doi:10.1016/j.jneumeth.2005.12.027
22. Lynch I, Salvati A, Dawson KA. Protein–nanoparticle interactions: what does the cell see? Nat Nanotechnol 2009; 4: 546–547; doi:10.1038/nnano.2009.248
23. Mailänder V, Lorenz MR, Holzapfel V, *et al*. Carboxylated superparamagnetic iron oxide particles label cells intracellularly without transfection agents. Mol Imag Biol 2008; 10: 138–146; doi:10.1007/s11307-007-0130-3
24. Schäfer R, Kehlbach R, Wiskirchen J, *et al*. Transferrin receptor upregulation: in vitro labeling of rat mesenchymal stem cells with superparamagnetic iron oxide. Radiology 2007; 244: 514–523; doi:10.1148/radiol.2442060599
25. De Cuyper M, Joniau M. Mechanistic aspects of the adsorption of phospholipids onto lauric acid stabilized magnetite nanocolloids. Langmuir 1991; 7: 647–652; doi:10.1021/la00052a010
26. De Cuyper M, Baert J, Cocquyt J, Van der Meeren P. A successful strategy for the production of cationic magnetoliposomes. Z Phys Chem 2006; 220: 133–141.
27. Soenen SJ, Brisson AR, De Cuyper M. Addressing the problem of cationic lipid-mediated toxicity: the magnetoliposome model. Biomaterials 2009; 30: 3691–3701; doi:10.1016/j.biomaterials.2009.03.040